Visible Light-Controlled Intracellular Synthesis of Supramolecular Peptide Nanostructures

Yong Ren[1], Zhixuan Zhou[1,2], Iain Harley[1], Özlem Aydin[1], Jiaqi Xing[1], Konrad Maxeiner, Ingo Lieberwirth[1], Katharina Landfester[1], David Y.W. Ng[1,*], Tanja Weil[1,*]

[1] Max Planck Institute for Polymer Research, 55128 Mainz, Germany

[2] State Key Laboratory of Chemo/Biosensing and Chemometrics, College of Chemistry and Chemical Engineering, Hunan University, Changsha 410082, PR China

* Corresponding Author. Email: weil@mpip-mainz.mpg.de; david.ng@mpip-mainz.mpg.de

Abstract

The complex dynamics and transience of supramolecular pathways in living cellular environments impede the correlation between diverse hierarchical species and their biological functions. The necessary breakthrough requires the precise control of supramolecular events at discrete time points via synthetic chemistry and their real-time visualization in native cells. Herein, we designed two peptide sequences that undergo a cascade of visible light-induced molecular and supramolecular transformations to form various assembly species in cells. In contrast to endogenous stimulus-responsive self-assembling systems, the irradiation with light enable full control over the reaction cascade where the monomer generation and concentration in turn regulates the assembly kinetics. Phasor-fluorescence lifetime imaging (phasor-FLIM) traced the formation of various assembly states in cells and revealed subsequent out-of-equilibrium dynamics associated with monomer activation and consumption. These temporally resolved assemblies show that the emergence of cytotoxicity is correlated to the accumulation of oligomers beyond the cellular efflux threshold.

Introduction

Optogenetic techniques have been transformative in cell biology, enabling the use of light as a trigger to initiate biochemical processes in living cells with high spatiotemporal resolution[1-3]. This enables the manipulation of neuronal function, gene expression and signaling in heterogeneous tissues using a combination of genetic engineering and light in a minimally invasive manner[4-6]. The technique relies on the expression of light-sensitive ion channels, enzymes or transcription factors to precisely

control biochemical signaling pathways by external light activation. More recently, the expression and light-activated assembly of aggregation-prone proteins, such as amyloids, succeeded in elucidating the framework involved in amyloid formation and its biochemical impact on living cells[7-9]. However, the drawback of expressing light-activated proteins is the inability to control local concentrations, i.e. of self-assembling amyloid proteins, which would be necessary to unravel the transformation dynamics, assembly kinetics and the impact of supramolecular defects on their biochemical properties. It would therefore be essential to control supramolecular assembly at discrete time points to characterize the formation of transient intermediates and stable assemblies.

The molecular pathways of peptide and protein assembly in cells and their impact on cellular function are being subject of intense research[10-19]. The classical model of amyloid self-assembly is based on monomer-by-monomer addition. Recently, it has been proposed that amyloid-like self-assembling peptides can undergo liquid-liquid phase separation prior to their self-assembly[20-22]. In this case, peptide-rich liquid droplets serve as nucleation precursors while intermediate species trigger nucleation, assembly and growth[23]. Challenges arise from the fact that many parameters direct the self-assembly pathways and the subsequent growth of the formed aggregates such as the stability and lifetime of the monomers and intermediates, their local concentrations, the nucleation barrier as well as temperature[24-29]. The heterogeneity of aggregates is further amplified by the formation of kinetically-driven metastable structures upon encountering different intracellular environments. As such, synthetic approaches that control the supply of active monomers to produce different assembly states and dynamics is necessary to provide the critical breakthrough in correlating aggregation-based function in living cells.

However, controlling monomer concentrations and supramolecular assembly in the living cellular environment is challenging due to the intricate processes of internalization, transport and localization[30]. Depending on the spatial localization, the crowded intracellular medium imposed by the high density of bio-macromolecules and organelles influences reaction kinetics [31, 32], while supramolecular interactions depend on how active molecules are transported intracellularly and locally enriched. As these parameters only exist in living cells and cannot be studied in model systems, in-situ technologies such as the use of phasor- fluorescence lifetime imaging (phasor-FLIM)

are invaluable for tracking dynamic self-assembly processes in real time using time-resolved fluorescence[33]. By combining photocleavable self-assembling peptides with phasor-FLIM imaging technology, we aim to understand how assembly is controlled, promoted and propagates in living cells.

In this study, we present the construction of two amphiphilic pro-assembling peptide sequences (**1**, **2**) protected by a visible light-sensitive cage group. The peptides are designed to undergo a cascade of visible light-induced molecular and supramolecular transformations to form nanofibers in the crowded environment of living cells (Fig. 1). Cell internalization of the caged peptides is facilitated by a cell membrane-penetrating oligo-arginine peptide sequence. The photolysis reaction and subsequent conversion of the stable photocaged monomers (**1**, **2**) into the "active" self-assembling peptides (**1a**, **2a**) was realized inside living cells upon irradiation with 505 nm visible light. In contrast to previously reported caged peptides that respond to endogenous stimuli such as pH or reactive oxygen species, the irradiation time now controls the uncaging reaction and thus monomer generation and concentration, which in turn regulates the assembly kinetics. A near-infrared (NIR) fluorophore has been attached to peptide **2** to allow tracking of the assembly dynamics, in particular the transition of different molecular and supramolecular species, using the recently reported phasor-FLIM technology. We report an intracellular synthesis strategy that encodes the molecular information for light sensitivity and fibril formation into the molecular structure of peptides to control and image different assembly states and dynamics of self-assembling peptide monomers, intermediates and nanofibers in living cells using visible light. Direct imaging of the complex assembly processes inside cells is correlated with their impact on cell viability.

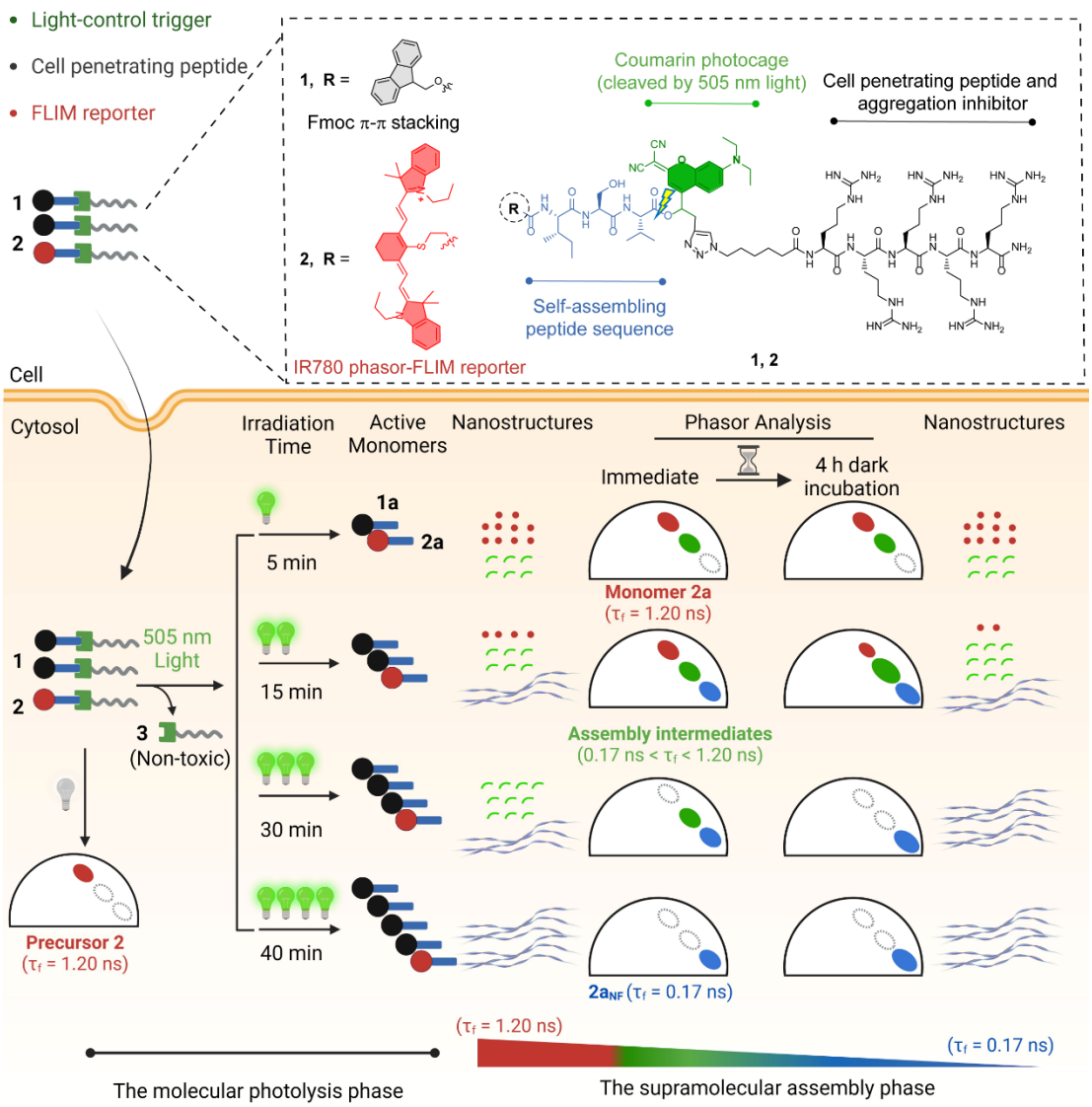

Fig. 1. Design of the photocaged pro-assembling peptide **1** and **2** encoded with the molecular information to form aggregates by light ("optoaggregates") inside cells and image the assembly process beyond the background emission of cells and the photocage. Pro-assembling peptide **1** and **2** (τ_f = 1.20 ns) entered A549 cells via "R_5"-mediated endocytosis. Visible light serves as an external stimulus to transform **1** and **2** to self-assembling peptide **1a** and **2a** upon irradiation. The assembly dynamics are monitored as photons change between τ_f = 1.20 ns and τ_f = 0.17 ns during assembly.

Design and synthesis of the photocaged pro-assembling peptides (1 and 2)

The photocleavable pro-assembling peptides (**1** and **2**) have been designed to contain four main functionalities: (1) the self-assembling peptide sequence (Fmoc-Ile-Ser-Val,

Fmoc-ISV) carrying (2) the IR780 chromophore as a phasor-FLIM reporter for intracellular imaging of the aggregation process; (3) the redshifted coumarin photocage that can be cleaved by 505 nm visible light and (4) a transporter peptide comprising five arginine (R_5) residues, whose polarity simultaneously prevents assembly and facilitates cellular uptake prior to irradiation. The proposed mechanism involves the initial internalization of the pro-assembling precursors (**1**, **2**) into cells supported by the R_5 sequence. Here, a co-assembly strategy is essential because **2a**, the photolysis product of precursor **2**, is unable to self-assemble into nanofibers, even at a high concentration of 100 µM (Fig. S24). After exposure to 505 nm light, the photocage is cleaved, leading to the release of the active self-assembling monomers (**1a**, **2a**), which co-assemble into NIR emitting nanofibers. The irradiation time allows controlling the generation of the self-assembling monomers (**1a**, **2a**) and their respective local concentrations. In this way, different assembly states as well as nanostructure formation can be regulated within cells.

The synthesis of precursors **1** and **2** involves a combination of solid-phase peptide synthesis (SPPS) and solution-phase methods. The photocage is synthesized in solution through multiple reaction steps (Fig. S1a), while the peptide components, including **Fmoc-ISV** and the R_5 peptide, are synthesized using SPPS (Fig. S1b and S1c). The conjugate of the photocage and R_5 are synthesized in solution via a copper-catalyzed azide–alkyne cycloaddition (CuAAC) reaction (Fig. S1d), followed by coupling with **Fmoc-ISV** using diisopropylcarbodiimide and 4-(dimethylamino)pyridine (Fig. S1e). Finally, all protecting groups are cleaved in the presence of 95% trifluoroacetic acid (TFA) to obtain precursors **1** and **2**, characterized by liquid chromatography–mass spectrometry (LC–MS) and matrix-assisted laser desorption ionization (MALDI)–MS (Fig. S20-23). The synthesis details are included in the Supporting Information (Fig. S1).

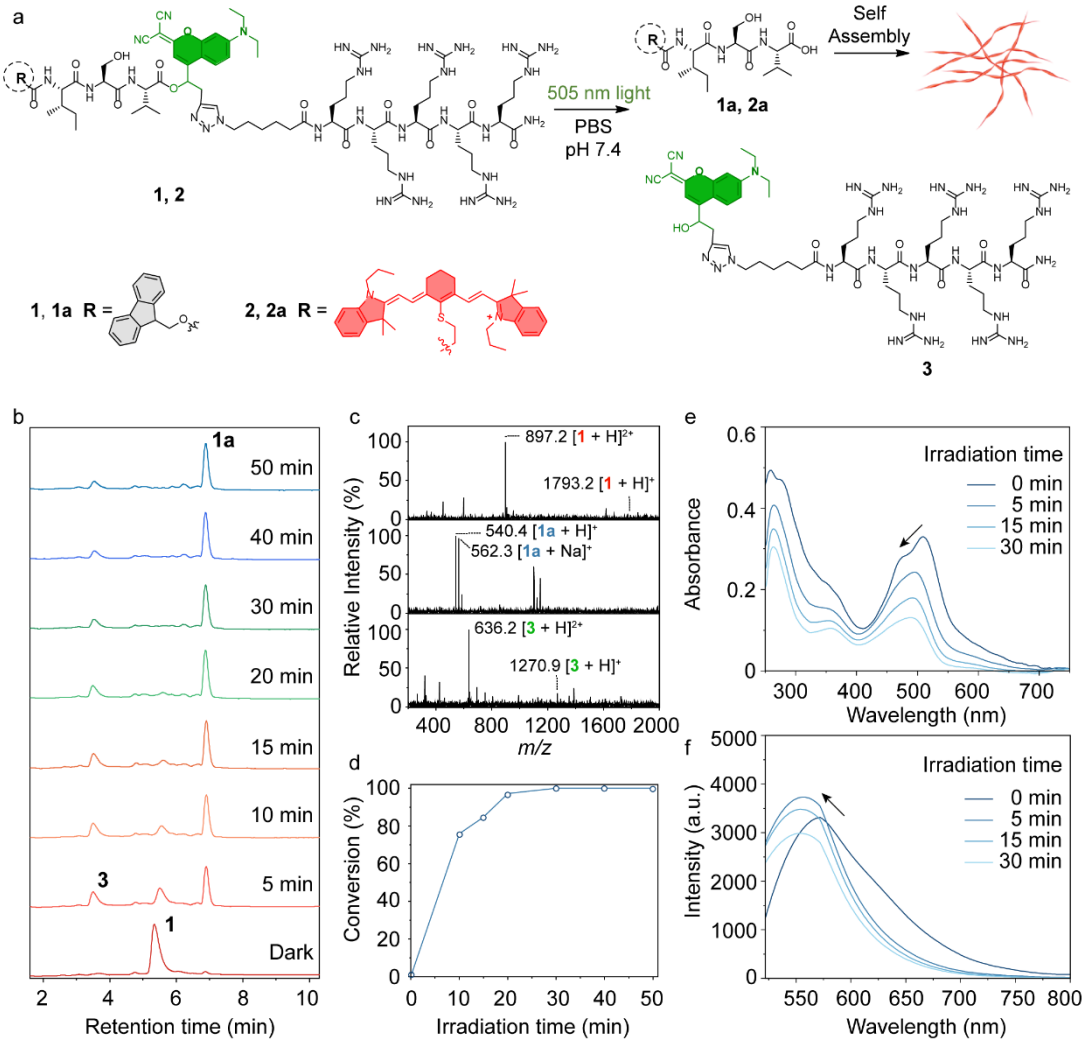

Fig. 2. (a) Molecular design and reaction scheme for all chemical transformations of photocaged peptides **1** and **2** (25 μM, ratio of **1**:**2** = 9:1) that assemble into nanofibers ("optoaggregates"). (b) LC-MS kinetic analysis for the photolysis reaction of **1** (25 μM) in NH_4HCO_3 buffer (pH 7.4, 20mM) upon irradiation with 505 nm visible light. (c) Convoluted MS spectra in the LC-MS analysis for compound **1** (t_R = 5.12-5.73 min) and corresponding products **1a** (t_R = 6.73-7.11 min) and **3** (t_R = 3.23-3.75 min) after photolysis. (d) The correlation between light-irradiation time and conversion. The connecting line is drawn only to aid visualization of the trend. (e) The changes of UV-vis absorption spectra of **1** (25 μM) in PB (pH 7.4, 50 mM) after irradiation for 5 min, 15 min, 30 min; (f) Changes in the fluorescence spectra of **1** (25 μM) in PB (pH 7.4, 50 mM) after irradiation for 5 min, 15 min, 30 min.

The photolysis reaction was optimized by LC-MS (Fig. 2b). In NH_4HCO_3 buffer (pH 7.4, 20 mM), precursor **1** remained stable for 24 h in the absence of light (Fig. S25). Upon light irradiation at 505 nm, the ester bond of **1** (25 μM) was hydrolyzed in aqueous

buffer (NH_4HCO_3 buffer, pH 7.4, 20 mM), resulting in the formation of self-assembling peptide **1a** and the released photocage-R_5 **3**. After 5 min, there was a significant consumption of **1**, accompanied by the emergence of two new peaks with retention times (t_R) of 6.91 min and 3.52 min, respectively, both exhibiting *m/z* values consistent with the chemical formula of **1a** (*m/z* = 540.4 for [**1a** + H]$^+$ and 562.3 for [**1a** + Na]$^+$) and **3** (*m/z* = 636.2 for [**3** + H] $^{2+}$ and 1270.9 for [**3** + H]$^+$) (Fig.2c). Extending the irradiation time to 20 minutes leads to a 98% conversion from **1** to **1a** while an irradiation of 30 minutes resulted in the complete disappearance of **1** (Fig. 2b, 2c and 2d). No further discernible effect on the photolysis process was observed if irradiation times were prolonged to 40 and 50 mins (Fig. 2b, 2d). To demonstrate that precursor **2** can also be cleaved by 505 nm light, the corresponding photolysis reaction kinetics were measured. The results indicated that the ester bond of **2** (2.5 μM) was completely hydrolyzed within 10 minutes of irradiation at 505 nm, resulting in the formation of peptide **2a** (Fig. S26).

The optical properties associated with the photolysis and self-assembly processes were then investigated. Precursor **1** exhibited an absorption band centered at 505 nm, characteristic of the coumarin chromophore. With increasing irradiation time, the absorption of the coumarin chromophore gradually decreased, accompanied by a slight hypsochromic shift (Fig. 2e). This shift can be attributed to the self-assembly behavior of **1a** in solution. The emission of the coumarin chromophore on the peptide initially exhibited a slight increase upon irradiation, probably due to its release from the peptide[34]. However, this was followed by a gradual decrease, which can be attributed to the self-assembly of **1a** in solution (Fig. 2f).

Light-induced Assembly Profile and Phasor-FLIM Calibration

The light-induced self-assembly and optoaggregate formation was initially studied by dynamic light scattering (DLS) analysis, which revealed a gradual increase in the sizes of the formed nanostructures over the irradiation times (Fig. 3d). Without irradiation, a 25 μM solution of **1** in PB (pH 7.4, 50 mM) remained soluble and exhibited no aggregation (Fig. 3d). After 1 min, nanometer sized aggregates were already formed that steadily increased and during 10 min of irradiation leading to the formation of micrometer sized aggregates (“optoaggregates”). The formation of the optoaggregates was imaged by time-dependent transmission electron microscopy (TEM) for similar irradiation times. Distinct nanofiber structures with increasing fiber densities occurred proportional to the irradiation time. Initially, a small number of fiber fragments were

observed after 5 min of irradiation. This was followed by a significant increase in fiber quantity after 15 min of irradiation (Fig. 3a, 3b). With prolonged irradiation to 30 min, the formation of denser nanofiber networks became apparent. Time-dependent cryogenic high-resolution TEM images confirmed the formation of similar nanostructures in solution upon light exposure (Fig. 3c). Interestingly, the image at 5 min presented the existence of discrete liquid droplets, potentially formed as a result of a liquid-liquid phase separation (LLPS) process. These droplets further convert to thermodynamically favorable nanofibers when more monomers were generated after longer irradiation time. Time-dependent circular dichroism (CD) analysis revealed an increasing signal at 203 nm (Fig. 3e), indicating the formation of ordered β– sheet secondary structures, which increased during irradiation. Additionally, the characteristic π→π* transition of the Fmoc group at 265 and 274 nm correlated positively with irradiation time, suggesting that the Fmoc group participates in the assembly. However, in the absence of irradiation, precursor **1** showed no obvious signal between 180 and 280 nm (Fig. S27). To validate the co-assembly behavior, co-assembled nanofibers (**1a** + **2a**, mol. ratio = 9:1) were prepared in DMEM and imaged using confocal laser scanning microscopy, revealing the presence of NIR emitting fibers, confirming the successful co-assembly process (Fig. S28). To calibrate the fluorescence lifetime profile under physiological conditions, the nanofibers were assembled in DMEM and transferred onto a culture of A549 lung adenocarcinoma cells. Herein, 0.1 eq. of peptide **2** with an IR780 dye as a phasor-FLIM reporter were used for co-assembly. The free molecule control was accomplished using non-irradiated **1**+**2** (mol. ratio = 9:1) in A549 cells. Phasor-FLIM analysis revealed that free molecules exhibited a fluorescence lifetime (τ_f) of 1.20 ns prior to irradiation (Fig. S29), whereas the assembled nanofibers revealed a τ_f ranging from 0.75 ns to 0.17 ns, representing different assembly states (Fig. 3f, 3g).

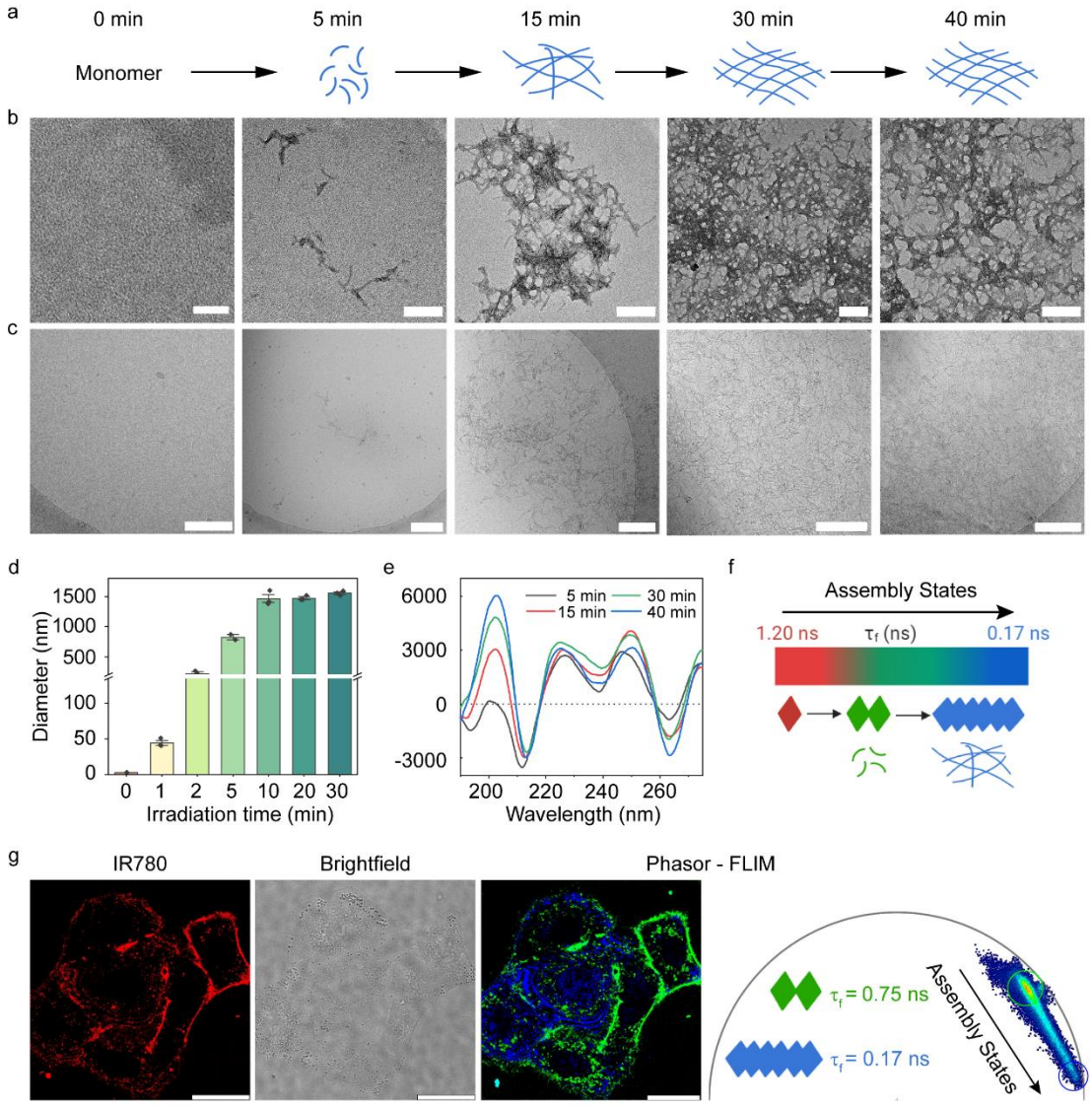

Fig. 3. Nanofibers formation observed in the light-induced self-assembly over time. (a) Scheme of light-induced peptide assembly and (b) corresponding TEM images of co-assembled (25 μM, ratio of **1**:**2** = 9:1) nanofibers formed at different irradiation time. Scale bar: 200 nm. (c) Corresponding cryogenic high-resolution TEM images of the co-assembled nanofibers (25 μM) in PB (pH 7.4, 50 mM) over time. Scale bar, 200 nm. (d) Dynamic light scattering kinetics analysis for the light-induced nanostructure formation of **1** (25 μM) in PB (pH 7.4, 50 mM) over time. Changes in diameter were measured. (e) CD kinetics analysis of **1** in a mixture of PB (pH 7.4, 100 mM) and MeOH (0.5 vol %) over irradiation time. (f) Schematic illustration of the assembly dynamics from monomers to assemblies, leading to decreased fluorescence lifetimes (1.20 ns to 0.75 ns to 0.17 ns) upon oligomerization and formation of the optoaggregates. (g) Fluorescence lifetime analysis of assembly progression out of A549 cells using phasor analysis. Two major species can be identified showing τ_f values of 0.75 ns (oligomers) and 0.17 ns

(larger assemblies, optoaggregates).

Visualization of the Light-induced Nanofiber Formation Process in Cells Using CLSM and Phasor-FLIM

The R_5-induced endocytosis into A549 lung alveolar adenocarcinoma cells was visualized using confocal laser scanning microscopy (CLSM) (Fig. S30). Different incubation times with 25 μM **1**+**2** (mol. ratio = 9:1), ranging from 2 h to 6 h, were tested to determine the optimal conditions for cellular uptake. After 4 h of incubation, peak cellular uptake was observed, as evidenced by both the green fluorescence from the coumarin dye and the NIR emission of IR780 (Fig. S30). To acquire an understanding of the assembly progression, we performed corresponding imaging using Phasor-FLIM. Cells were pre-treated with **1**+**2** for 4 h, followed by washing off the excess extracellular precursors. Subsequently, the cells were subjected to irradiation for 5 min, 10 min, 15 min, 30 min and 40 min, followed by immediate phasor-FLIM imaging (Fig. 4d-4i). The progression of aggregation over time can be tracked by the shifting of photon populations between two characteristic phasors on the phasor plot, representing monomers and assemblies (Fig 4e-4i). In the absence of light, the precursors exhibited a homogenous, single-component fluorescence decay with τ_f = 1.20 ns (Fig. S31). Upon irradiation, the photocaged peptides (**1** and **2**) generated the corresponding active monomers (**1a** and **2a**), which subsequently self-assembled into nanofibers exhibiting a decreased τ_f. After 5 min of irradiation, the phasor analysis showed intracellular photons exhibiting fluorescence lifetimes of 1.20 ns > τ_f > 0.75 ns indicating that the major component were still monomers and first traces of assembled species were observed (Fig. 4e). Supported by TEM and cryo-TEM images, after 5 min of irradiation, only monomers were produced at a low concentration, and the formation of oligomers occurred but no further progression into mature nanofibers was observed (Fig. 3b, 3c). When increasing the irradiation time to 10 min, morphological changes of the cells were detected (Fig. 4c) along with the emergence of a new photon population with τ_f = 0.17 ns, indicative of the formation of nanofibers (Fig. 4f). Extending the irradiation time to 15 minutes lead to a further consumption of the generated monomers and the concomitant formation of oligomers and assemblies (Fig. 4g). Upon 30-min of irradiation, the pool of intracellular precursors was fully consumed and corresponding population of photons shifting to τ_f = 0.17 ns increased significantly, implying the progression of most supramolecular species into assemblies (Fig. 4h). Finally, irradiation for 40 min resulted in the complete transformation of the photocaged

peptides into assemblies (Fig. 4i). As irradiation time increased, notable morphological changes in the cells were observed (Fig. 4c). Therefore, a time-dependent cell viability assay was conducted, revealing that 30 min of irradiation in the presence of **1** and **2** reduced cell viability to approximately 37% under these conditions (Fig. S32). This suggests that the assembly formation need to reach a critical point to induce significant cytotoxicity.

To rule out the possibility that the cytotoxicity observed was due to the phototoxicity of 505 nm light, the phototoxic effect of IR780 dye or the byproduct of photolysis **3**, pertinent experiments were conducted. Initially, phototoxicity from the light source was assessed by conducting cell viability assays and confocal imaging on untreated cells (Fig. S33, S36), revealing that light (505 nm wavelengths) induced no significant toxicity to A549 cells. Furthermore, to investigate the potential cytotoxic effects induced by both the phototoxic effect of IR780 dye and **3**, cell viability was studied on A549 cells treated with **2** at a concentration of 2.5 μM used for co-assembly, and **3** at 25 μM (Fig. S36), with and without 30-minute irradiation. Additionally, confocal imaging was performed for each corresponding treatment (Fig. S34, S35). The results clearly indicated that both compounds did not induce damage to A549 cells (Fig. S34-36). Therefore, it can be concluded that the observed cytotoxicity solely resulted from the formation of nanostructures induced by light.

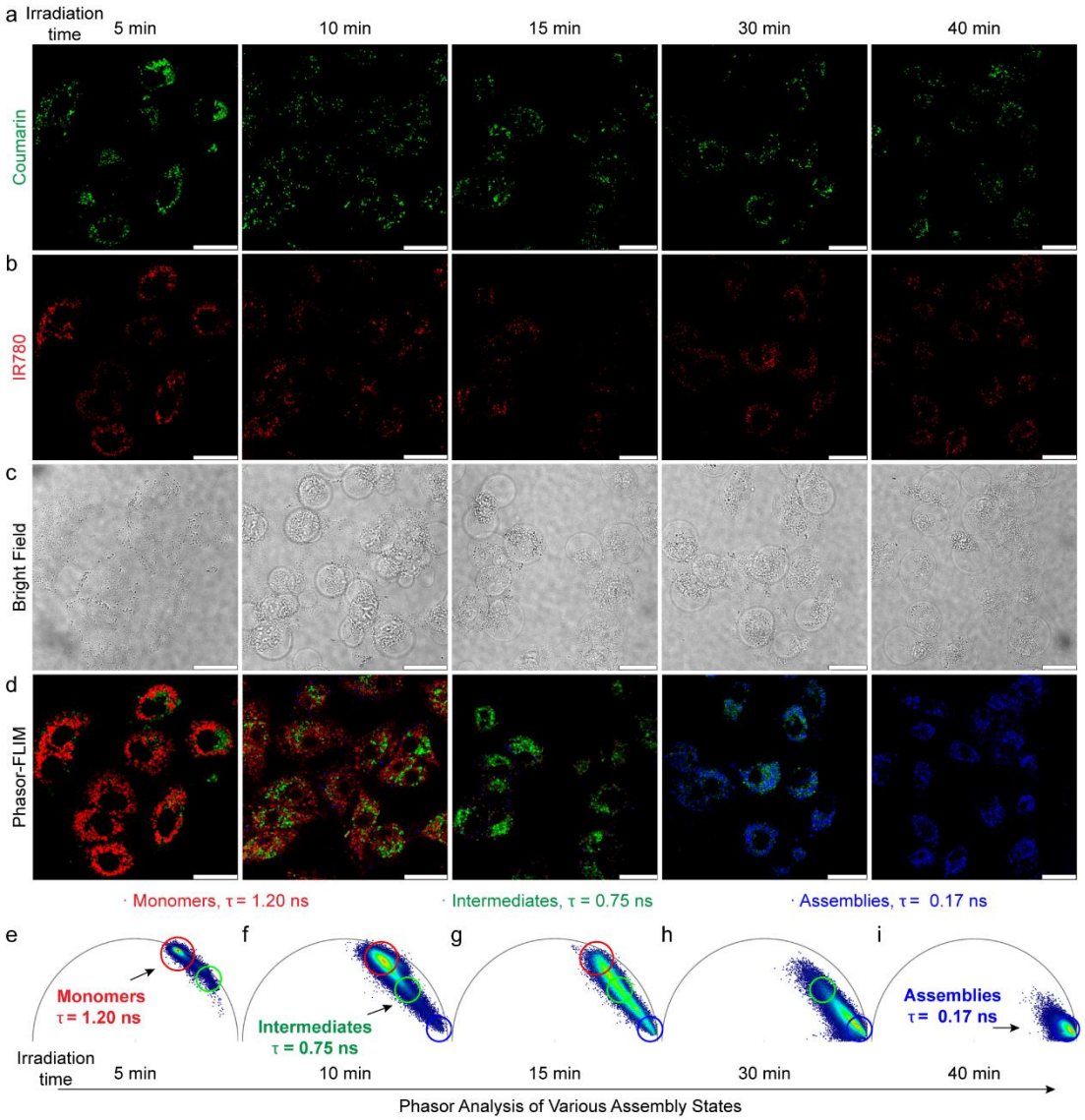

Fig. 4. Time-lapsed phasor-FLIM analysis of **1** and **2** internalization and assembly states upon different irradiation times. Time-dependent fluorescence of coumarin (a) and IR780 (b), brightfield (c), and phasor-FLIM images (d) of A549 cells treated with **1** and **2** (25 μM, ratio of **1**:**2** = 9:1). Bottom row: Phasor maps of A549 cells treated with **1** and **2** (25 μM, ratio of **1**:**2** = 9:1) upon different irradiation times, including 5 min (e), 10 min (f), 15 min (g), 30 min (h) and 40 min (i). Arrows indicate that the irradiation results in chemical photolysis and the nanostructure formation and growth with a concomitant change in the phasor-FLIM. Scale bars, 25 μm.

Temporal Analysis of Precisely Controlled Nanofiber Formation in Cells Using Phasor-FLIM

In contrast to endogenous stimulus-responsive self-assembling systems, the light-triggered assembly offers a unique opportunity to control the assembly kinetics within

cells by modulating the intracellular concentration of the active monomers. The kinetics involved consist of two distinct phases: the molecular photolysis phase, generating the "active" self-assembling monomers, and the supramolecular assembly phase, during which nuclei are formed that progress to oligomers and mature fibers[35]. At the molecular level, the photolysis reaction regulates the generation and local concentration of the active monomers that proceed into the self-assembly phase. During assembly, active monomers are consumed relative to their local concentration, which determines the nanostructure formation process. When the local concentration is below the critical aggregation concentration (CAC), assembly does not start and no nanostructures are formed. Conversely, when the concentration of active monomers exceeds the CAC, the production and consumption rates determine the extent of nanostructure formation. If the photolysis production rate of active monomers exceeds their assembly consumption rate, the excess of the active monomers will continue to undergo assembly even after the light has been switched off, causing a loss in temporal precision of the supramolecular polymerization process. To demonstrate these limits, we conduct an extensive analysis of assembly processes and subsequent biological effects on A549 cells (Fig. 5). Following identical 4 h peak internalization, the cells were exposed to light for 5 min, 10 min, 15 min and 30 min, respectively, corresponding to the photolysis conversion of the photocaged precursors (**1** and **2**) in cell-free conditions (Fig. 2d), to control the amount of active monomers that then progressed into the subsequent assembly process. This was followed by a dark incubation period of 1 to 4 hours, during which we examined the assembly progression and the associated biological effects using phasor analysis and cell viability assays (Fig. 5a-h).

With an irradiation time of 5 min, subsequent incubation in the dark for 1-4 h did not show further progression on the phasor plot (Fig. 5a, Fig. S38). Phasor analysis revealed that the population of photons remained 1.20 ns > τ_f > 0.75 ns, indicating that the concentration of active monomers surpassed the critical aggregation concentration (CAC), therefore leading to nucleation. However, it did not reach a critical concentration threshold for propagation. After irradiation for 10 min, 1 h incubation in the dark led to increase in nucleation (Fig. 5b), whereas after 4 h, most monomers were consumed (Fig. 5b, Fig. S39). The results indicated that 10 min of irradiation is sufficient to produce the active monomers in excess that continued to fuel the assembly process even during the dark phase when the light was switched off. Extending the irradiation to 15 min yielded even more noteworthy changes of phasor plots (Fig. 5c, Fig. S40).

Incubation for 4 h resulted in the increase of the population of photons shifting to 0.75 ns > τ_f > 0.17 ns, indicative of a higher consumption of monomers, further progression into oligomers and the subsequent propagation into a larger number of assemblies compared to the 10 min irradiation experiment (Fig. S40). Compared to 10 min irradiation, 15 min irradiation generated a considerably higher light-induced uncaging, producing higher monomer concentrations, which further promoted the supramolecular nucleation process and subsequently propagated to nanofibers within the same timeframe.

Furthermore, 30 min irradiation led to complete consumption of the active monomers, with photon populations of 0.75 ns > τ_f > 0.17 ns, corresponding to the formation of a substantial number of assemblies and the presence of a small number of oligomers. 2 h of incubation led to significant increase in assembly propagation and 3 h incubation resulted in the complete transformation of the active monomers and oligomers into assemblies (Fig. 5d, Fig. S41). The observation indicated that the formation of a substantial amount of assemblies facilitated the propagation of all remaining oligomers, thereby driving the assembly process to completion. Overall, these findings demonstrated that during assembly, when the photolysis production rate of monomers exceeds their assembly consumption rate, the excess monomers or unconsumed oligomers continue to contribute towards the assembly process even after the cessation of light exposure. In total, our strategy enables to effectively govern the molecular photolysis phase to generate accurate concentrations of active monomers that contributes towards the self-assembly phase, which remains unattainable with assembly systems induced by endogenous stimuli. Additionally, the photocaged pro-assembling peptides offer a unique opportunity to visualize and unravel supramolecular assembly processes inside living cells, which will be crucial for the formation of artificial nanostructures, compartments or synthetic organelles, an area of emergent importance.

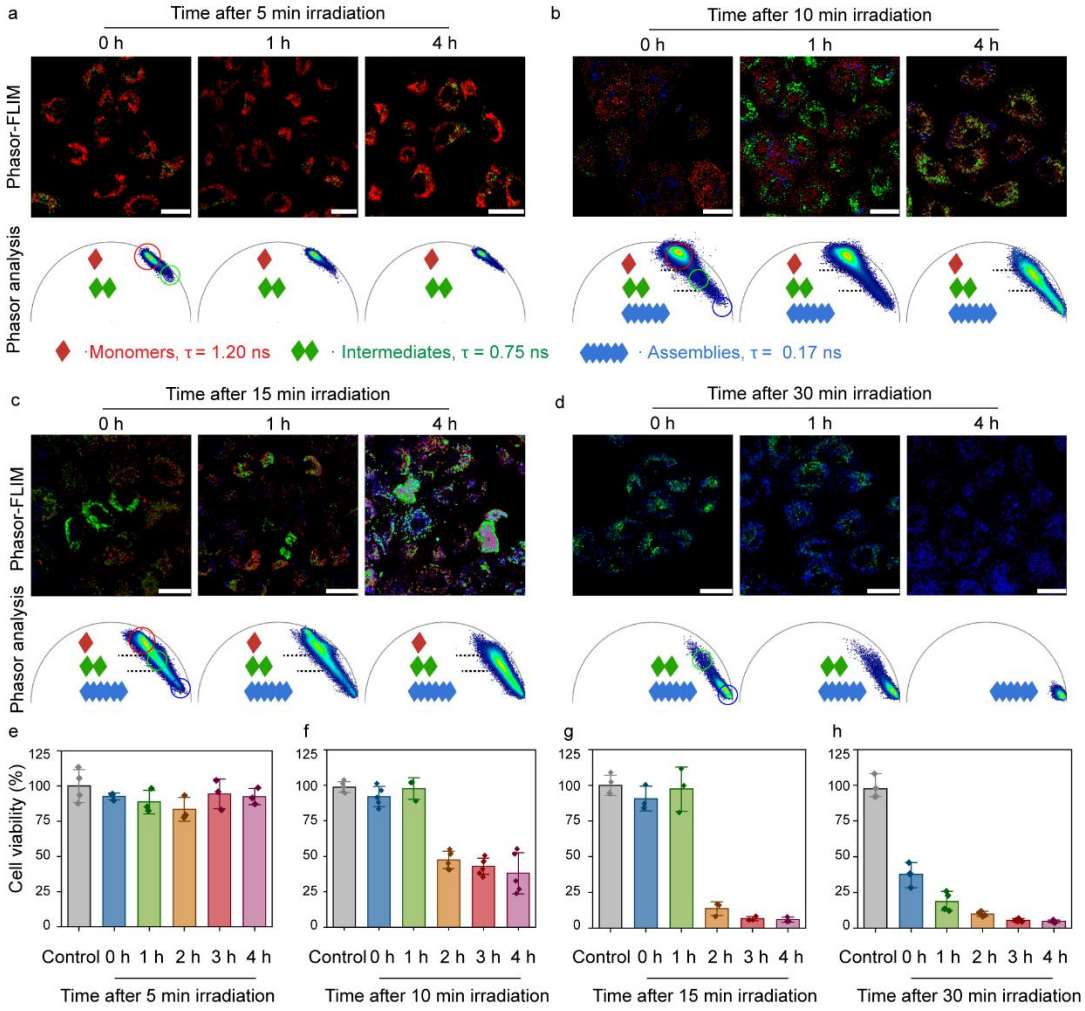

Fig. 5. Phasor-FLIM analysis and cell viability study of various assembly states and dynamics for 1-4 h incubation after different irradiation times. Phasor-FLIM analysis of A549 cells for 1-4 h incubation after irradiation for 5 min (a), 10 min (b), 15 min (c), 30 min (d). Cell viability study for A549 cells for 1-4 h incubation after irradiation for 5 min (e), 10 min (f), 15 min (g), 30 min (h). Scale bars, 25 μm.

Inspired by the finding that the assembly phase would be continuously fueled by the over-production of active monomers, even after the light has been switched off, we hypothesized that associated cytotoxicity due to the accumulation of oligomers will see a delayed response. To investigate whether the species that were dynamically formed during supramolecular assembly correlate with the corresponding biological effects, cell viability was examined as a function of post-illumination assembly. Interestingly, 5 min of irradiation did not result in significant toxicity towards A549 cells even after 4 h of incubation (Fig. 5e).

However, 10 min of irradiation did not induce significant toxicity within the first hour of incubation, but resulted in an approximately 50% decrease in cell viability between 2 h and 4 h (Fig. 5f). In addition, 15 min of irradiation resulted in higher toxicity, reducing cell viability to 10% after 2 h (Fig. 5g). After 30 min of light exposure, cell viability immediately decreased to approximately 37%, ultimately dropping to less than 5% after 4 h (Fig. 5h).

By integrating the cellular effects with phasor analysis and the LLPS-mediated supramolecular pathway (Fig. 6), it is evident that during the early stages of assembly, the formation of peptide-rich liquid droplets and oligomers does not induce significant cytotoxicity. However, as these oligomers accumulated and further propagated into larger assemblies, notable cytotoxic effects emerge. These effects are correlated with the quantity of assemblies; specifically, greater numbers of assembles result in more pronounced cellular toxicity.

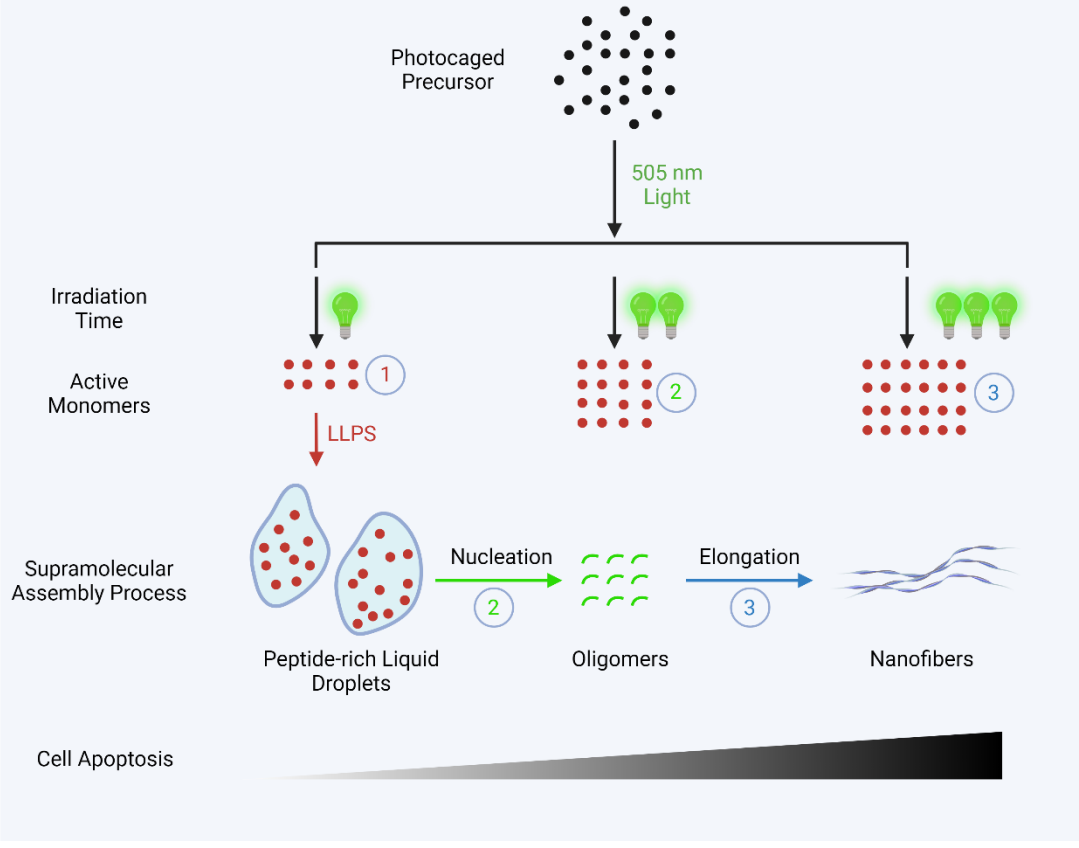

Fig. 6. Illustration of LLPS-mediated supramolecular assembly pathway and its correlation with cellular effects. The liquid-liquid phase separation (LLPS) into peptide-rich liquid droplets is a critical step prior to the nucleation of supramolecular nanofibers. The cellular toxicity results show the formation of liquid droplets and oligomers did not induce significant cell toxicity. After further elongation into nanofibers, observable cytotoxic effects emerge.

Conclusion

In conclusion, we present photocaged pro-assembling peptides to control and image visible light-induced supramolecular assembly inside complex cellular environments. In combination with advanced imaging technologies, precise control over the generation of diverse assembly states and real-time imaging of these processes was achieved. By integrating imaging and relevant biological assays, we discovered that during the initial stage of peptide assembly, the formation of oligomers did not lead to observable cytotoxic effects. Significant cytotoxicity was observed only upon the formation of sufficient quantities of the supramolecular assemblies. Furthermore, by performing phasor analysis on A549 cells post-irradiation, we have elucidated the intricate dynamics of assembly in greater detail in cells. The observation highlighted that the concentration, production rate, and consumption rate of monomers significantly influence assembly dynamics inside cells. While precise control over the molecular phase of photolysis is achievable, managing the supramolecular phase becomes challenging when the production rates of monomers exceed their consumption rates. Time-dependent cell viability analysis revealed that the cytotoxic effects are closely correlated with the quantities of nanostructures formed intracellularly. Our study facilitates precise control over supramolecular events at discrete time points, and the new imaging technologies offer deeper insights into the dynamic assembly processes with native cells. Our results will pave the way to address grand challenges in supramolecular drug discovery and relevant biomedical research.

Acknowledgements

The authors gratefully acknowledge financial support from the Max Planck-Bristol Center for Minimal Biology and the Deutsche Forschungsgemeinschaft (DFG, German Research Foundation) – Projektnummer 464588647 (SFB1551 R04), Projektnummer 213555243 (SFB 1066 B16). Y.R. and J.X. thanks the China Scholarship Council for a fellowship. Z.Z. is supported by the Alexander von Humboldt Foundation.

Reference

1. Emiliani, V. *et al.* Optogenetics for light control of biological systems. *Nature Reviews Methods Primers* **2**, 55 (2022).
2. Gradinaru, V., Mogri, M., Thompson, K.R., Henderson, J.M. & Deisseroth, K. Optical Deconstruction of Parkinsonian Neural Circuitry. *Science* **324**, 354-359 (2009).

3. Deisseroth, K. Optogenetics: 10 years of microbial opsins in neuroscience. *Nature Neuroscience* **18**, 1213-1225 (2015).
4. Kim, C.K., Adhikari, A. & Deisseroth, K. Integration of optogenetics with complementary methodologies in systems neuroscience. *Nature Reviews Neuroscience* **18**, 222-235 (2017).
5. Kravitz, A.V. *et al.* Regulation of parkinsonian motor behaviours by optogenetic control of basal ganglia circuitry. *Nature* **466**, 622-626 (2010).
6. Nzigou Mombo, B. *et al.* Reversible photoregulation of cell-cell adhesions with opto-E-cadherin. *Nature Communications* **14**, 6292 (2023).
7. Zhang, A., Zhao, S., Tyson, J., Deisseroth, K. & Bao, Z. Applications of synthetic polymers directed toward living cells. *Nature Synthesis* **3**, 943-957 (2024).
8. Sun, S., Liang, H.-W., Wang, H. & Zou, Q. Light-Triggered Self-Assembly of Peptide Nanoparticles into Nanofibers in Living Cells through Molecular Conformation Changes and H-Bond Interactions. *ACS Nano* **16**, 18978-18989 (2022).
9. Mueller, M., Rasoulinejad, S., Garg, S. & Wegner, S.V. The Importance of Cell–Cell Interaction Dynamics in Bottom-Up Tissue Engineering: Concepts of Colloidal Self-Assembly in the Fabrication of Multicellular Architectures. *Nano Letters* **20**, 2257-2263 (2020).
10. Zhou, Z. *et al.* In Situ Assembly of Platinum(II)-Metallopeptide Nanostructures Disrupts Energy Homeostasis and Cellular Metabolism. *Journal of the American Chemical Society* **144**, 12219-12228 (2022).
11. Chagri, S., Ng, D.Y.W. & Weil, T. Designing bioresponsive precursors to build synthetic functional assemblies inside living cells. *Nat. Rev. Chem.*, in press (2021).
12. Hu, B. *et al.* Noncanonical Amino Acids for Hypoxia-Responsive Peptide Self-Assembly and Fluorescence. *Journal of the American Chemical Society* **143**, 13854-13864 (2021).
13. Chang, R., Zhao, L., Xing, R., Li, J. & Yan, X. Functional chromopeptide nanoarchitectonics: molecular design, self-assembly and biological applications. *Chemical Society Reviews* **52**, 2688-2712 (2023).
14. Liu, Z., Guo, J., Qiao, Y. & Xu, B. Enzyme-Instructed Intracellular Peptide Assemblies. *Accounts of Chemical Research* **56**, 3076-3088 (2023).
15. Ulijn, R.V. & Smith, A.M. Designing peptide based nanomaterials. *Chemical Society Reviews* **37**, 664-675 (2008).
16. Chen, N. *et al.* Sulfatase-Induced In Situ Formulation of Antineoplastic Supra-PROTACs. *Journal of the American Chemical Society* **146**, 10753-10766 (2024).
17. Newcomb, C.J. *et al.* Cell death versus cell survival instructed by supramolecular cohesion of nanostructures. *Nature Communications* **5**, 3321 (2014).
18. Lee, S.S. *et al.* Sulfated glycopeptide nanostructures for multipotent protein activation. *Nature Nanotechnology* **12**, 821-829 (2017).
19. Sheehan, F. *et al.* Peptide-Based Supramolecular Systems Chemistry. *Chemical Reviews* **121**, 13869-13914 (2021).
20. Yuan, C. *et al.* Nucleation and Growth of Amino Acid and Peptide Supramolecular Polymers through Liquid–Liquid Phase Separation. *Angewandte Chemie International Edition* **58**, 18116-18123 (2019).
21. Levin, A. *et al.* Biomimetic peptide self-assembly for functional materials. *Nature*

Reviews Chemistry **4**, 615-634 (2020).
22. Wei, G. *et al.* Self-assembling peptide and protein amyloids: from structure to tailored function in nanotechnology. *Chemical Society Reviews* **46**, 4661-4708 (2017).
23. Levkovich, S.A., Gazit, E. & Laor Bar-Yosef, D. The Metabolostasis Network and the Cellular Depository of Aggregation-Prone Metabolites. *Angewandte Chemie International Edition* **62**, e202217622 (2023).
24. Ng, D.Y.W. *et al.* Directing intracellular supramolecular assembly with N-heteroaromatic quaterthiophene analogues. *Nature Communications* **8**, 1850 (2017).
25. Zhou, Z., Maxeiner, K., Ng, D.Y.W. & Weil, T. Polymer Chemistry in Living Cells. *Accounts of Chemical Research* **55**, 2998-3009 (2022).
26. Korevaar, P.A. *et al.* Pathway complexity in supramolecular polymerization. *Nature* **481**, 492-496 (2012).
27. Jonkheijm, P., van der Schoot, P., Schenning, A.P.H.J. & Meijer, E.W. Probing the Solvent-Assisted Nucleation Pathway in Chemical Self-Assembly. *Science* **313**, 80-83 (2006).
28. Roth, P. *et al.* Supramolecular assembly guided by photolytic redox cycling. *Nature Synthesis* **2**, 980-988 (2023).
29. Korevaar, P.A., Newcomb, C.J., Meijer, E.W. & Stupp, S.I. Pathway Selection in Peptide Amphiphile Assembly. *Journal of the American Chemical Society* **136**, 8540-8543 (2014).
30. Pieszka, M. *et al.* Controlled Supramolecular Assembly Inside Living Cells by Sequential Multistaged Chemical Reactions. *Journal of the American Chemical Society* **142**, 15780-15789 (2020).
31. Hansen, M.M.K. *et al.* Macromolecular crowding creates heterogeneous environments of gene expression in picolitre droplets. *Nature Nanotechnology* **11**, 191-197 (2016).
32. Ellis, R.J. Macromolecular crowding: an important but neglected aspect of the intracellular environment. *Current Opinion in Structural Biology* **11**, 114-119 (2001).
33. Ren, Y. *et al.* Supramolecular Assembly in Live Cells Mapped by Real-Time Phasor-Fluorescence Lifetime Imaging. *Journal of the American Chemical Society* **146**, 11991-11999 (2024).
34. Gandioso, A., Cano, M., Massaguer, A. & Marchán, V. A Green Light-Triggerable RGD Peptide for Photocontrolled Targeted Drug Delivery: Synthesis and Photolysis Studies. *The Journal of Organic Chemistry* **81**, 11556-11564 (2016).
35. Yuan, C., Li, Q., Xing, R., Li, J. & Yan, X. Peptide self-assembly through liquid-liquid phase separation. *Chem* **9**, 2425-2445 (2023).